encit 2020

ABCM Associação Brasileira de Engenharia e Ciências Mecânicas

18th Brazilian Congress of Thermal Sciences and Engineering
November 16–20, 2020 (Online)

ENC-2020-0291
ROTATIONAL EFFECTS ON THE SPANWISE PERIODIC FLOW OVER A WIND TURBINE AIRFOIL

Daniel Sampaio Souza
Elmer Mateus Gennaro
UNESP - São Paulo State University, Campus São João da Boa Vista, Av. Isette Correa Fontão, 505, São João da Boa Vista, SP 18976-750, Brazil
daniel.s.souza@unesp.br
elmer.gennaro@unesp.br

Abstract. *The effect of rotation on the steady flow field around a wind turbine airfoil is studied using computational fluid dynamics. Periodicity is imposed in the spanwise direction in order to disregard the influence of the three-dimensional geometric features of the full blade. The Reynolds-averaged Navier-Stokes equations are solved with the open source platform OpenFOAM. Simulations for two rather high angles of attack confirm the separation delay predicted by theoretical boundary-layer investigations. A lift increase of more than 60% is observed for an angle of attack of 16° and the predicted effect of rotation on the drag depends on the angle of attack considered. Interestingly, the model predicts a reduction of the recirculation region's volume, although no significant spanwise gradient of the flow field is observed. In summary, the model seems to be a viable tool to investigate the underlying physics of the rotational augmentation phenomenon.*

Keywords: *Aerodynamics, Wind energy, HAWT, Rotational augmentation, Finite volume method*

1. INTRODUCTION

At high local angles of attack, sections of rotating wings often experience loads greater than expected from two-dimensional data for the same angle of attack. Rotational effects change the behavior of the suction-side boundary layer at the inboard sections of rotor blades (Dwyer and McCroskey, 1970). As the sectional lift coefficient may achieve values beyond the maximum predicted for 2D conditions (Ronsten, 1992), rotating-wing aerodynamic tools must properly account for these effects in order to contribute to the design of efficient and reliable blades.

Different influence mechanisms of the rotational effects on the boundary layer have been identified. One mechanism is the delay of the boundary layer separation. Numerical solutions of the integral equations for three-dimensional boundary layer subjected to adverse pressure gradient by Banks and Gadd (1963) and Du and Selig (2000) showed that the rotation may shift the separation point downstream or even suppress the separation for mild pressure gradients. The separation delay was explained by the addition of streamwise momentum by the Coriolis force acting on fluid elements streaming in the spanwise direction due to the centrifugal force (Du and Selig, 2000). Separation delay accompanied by lift augmentation was also identified by Navier-Stokes simulations of the flow over wind turbine blades (Narramore and Vermeland, 1992; Hu *et al.*, 2006). Gross *et al.* (2012) suggested an alternative explanation for separation delay: streamwise vortices associated to crossflow instability change the transition process, anticipating the admission of fluid from outside the boundary layer and thus injecting streamwise momentum in the boundary layer at earlier boundary-layer stages.

However, rotational augmentation was also observed in the presence of significant flow separation. In fact, the highest levels of lift augmentation in comparison to 2D data were observed for conditions where a separation region of considerable size was present. For a highly turbulent freestream flow, measurements by Sicot *et al.* (2008) showed a significant increase of the lift coefficient of wind-turbine blade sections compared to two-dimensional flow, although no appreciable change of the boundary layer separation point was observed. Schreck and Robinson (2003) analyzed the state of the boundary layer based on unsteady pressure measurements acquired from real scale wind tunnel tests (Hand *et al.*, 2001). They observed that large increases of the sectional normal force compared to 2D flow were associated with the combined presence of a separation and reattachment on the section upper surface. Integral boundary-layer analysis by Dumitrescu *et al.* (2007) and Navier-Stokes simulations by Schreck *et al.* (2007) captured a standing spanwise vortical structure which may be associated to the pattern observed by Schreck and Robinson (2003). Mauro *et al.* (2017) argued that this structure is associated with the radial component of the Coriolis force. It is often argued that a radial pumping promoted by radial gradients of pressure and centrifugal acceleration (the term centrifugal pumping is often used) drains fluid from the recirculation region of inboard sections towards the blade tip, transporting mass and vorticity outboard (Jardin and David, 2014; Jardin, 2017). In such conditions it is observed that the volume of the separation region on inboard sections

is reduced in comparison to corresponding 2D flows (Chaviaropoulos and Hansen, 2000; Lanzafame *et al.*, 2015; Zhang and Deng, 2019), which may reduce the decamber effect of the separated boundary layer (Bangga *et al.*, 2017b).

Most commonly the studies of rotational effects on the flow over blade sections are based on data extracted from full rotating blades (Carcangiu *et al.*, 2007; Herráez *et al.*, 2014; Bangga *et al.*, 2017a). This approach have been greatly contributing to understand the underlying physics of rotational augmentation. Nevertheless, it does not allow us to rule out the effect of three-dimensional geometric characteristics of the blade on the sectional aerodynamics. Exceptionally, Chaviaropoulos and Hansen (2000) and Gross *et al.* (2012) considered sectional flows which were independent of a particular blade geometry. However, the former neglected all radial derivatives of the primitive variables and the latter was interested in the transition process, restricting the analysis to low angles of attack.

The work described here applies a three-dimensional computational fluid dynamics model, imposing periodicity in the spanwise direction, to study the flow field around an airfoil designed for wind turbine application subjected to rotational effects. The model is similar to the one proposed by Gross *et al.* (2012). However, the aim here is to investigate the effect of rotation mainly on separated flow condition. Therefore, the flowfield for two rather high angles of attack is examined for different values of the ratio between the chord and the radial position, which for some conditions is representative of the ratio between the Coriolis and the inertial force.

2. NUMERICAL MODEL

The aim is to represent the flow over a blade section at a distance R from the axis of a rotor at constant angular velocity $\mathbf{\Omega} = \Omega \mathbf{e}_y$, where $\mathbf{e}_y$ is the unit vector in the axial direction (see Fig. 1). For this, the governing equations for steady incompressible flow in cylindrical coordinates for a reference frame rotating with the blade are considered in non-dimensional form

$$Ro\frac{V_r}{r} + Ro\frac{\partial V_r}{\partial r} + \frac{\partial V_\theta}{r\partial\theta} + \frac{\partial V_y}{\partial y} = 0,$$

$$RoV_r\frac{\partial V_\theta}{\partial r} + V_\theta\frac{\partial V_\theta}{r\partial\theta} + V_y\frac{\partial V_\theta}{\partial y} + Ro\frac{V_rV_\theta}{r} =$$
$$-\frac{\partial p}{r\partial\theta} + \frac{1}{Re}\left(\frac{1}{r}\frac{\partial V_\theta}{\partial r} + \frac{\partial^2 V_\theta}{\partial r^2} + \frac{\partial^2 V_\theta}{r^2\partial\theta^2} + \frac{\partial^2 V_\theta}{\partial y^2} - \frac{V_\theta}{r^2} + 2Ro\frac{1}{r}\frac{\partial V_r}{r\partial\theta}\right) + 2Ro^2V_r,$$

$$RoV_r\frac{\partial V_y}{\partial r} + V_\theta\frac{\partial V_y}{r\partial\theta} + V_y\frac{\partial V_y}{\partial y} = -\frac{\partial p}{\partial y} + \frac{1}{Re}\left(\frac{1}{r}\frac{\partial V_y}{\partial r} + \frac{\partial^2 V_y}{\partial r^2} + \frac{\partial^2 V_y}{r^2\partial\theta^2} + \frac{\partial^2 V_y}{\partial y^2}\right),$$

$$RoV_r\frac{\partial V_r}{\partial r} + V_\theta\frac{\partial V_r}{r\partial\theta} + V_y\frac{\partial V_r}{\partial y} - \frac{1}{Ro}\frac{V_\theta^2}{r} =$$
$$-\frac{1}{Ro}\frac{\partial p}{\partial r} + \frac{1}{Re}\left(\frac{1}{r}\frac{\partial V_r}{\partial r} + \frac{\partial^2 V_r}{\partial r^2} + \frac{\partial^2 V_r}{r^2\partial\theta^2} + \frac{\partial^2 V_r}{\partial y^2} - \frac{V_r}{r^2} - \frac{2}{Ro}\frac{1}{r}\frac{\partial V_\theta}{r\partial\theta}\right) - 2V_\theta + Ro\, r,$$

where $r = r^*/c$ is the radial coordinate, $V_r = V_r^*/(\Omega c)$, $(V_\theta, V_y) = (V_\theta^*, V_y^*)/U$ are the velocity components, $p = p^*/(\rho U^2)$, U is the freestream velocity for the considered section and $(\partial r, r\partial\theta, \partial y) = (\partial r^*, r^*\partial\theta, \partial y^*)/c$ is a displacement of infinitesimal length. Note that superscript * denotes dimensional variables. The relevant non-dimensional numbers are the chord-based Reynolds number $Re = Uc/\nu$, where ν is the kinematic viscosity, the rotation number $Ro = \Omega c/U$, and the chord to radius ratio c/R.

To be able to assume periodicity in the spanwise direction, the analysis must be restricted. First, we must map the azimuthal increment of length $rd\theta$ to a straight line, whose length will be referred to as dx. For this to be reasonable, the curvature effects must be negligible, which is true for low values of c/R. On the other hand, in the limit $c/R \to 0$, the rotational effects disappear, and the flow is the one over an airfoil in linear motion. Therefore, following the approach proposed by Gross *et al.* (2012), the curvature effects were neglected by dropping all terms proportional to r^{-1} and r^{-2} from the governing equations, except those $\mathcal{O}(V_\theta/r)$, since the azimuthal velocity component is proportional to r. With these simplifications, and replacing radial displacements dr by spanwise displacements dz, the governing equations can be rewritten

$$\frac{\partial V_x}{\partial x} + \frac{\partial V_y}{\partial y} + Ro\frac{\partial V_z}{\partial z} = 0, \tag{1}$$

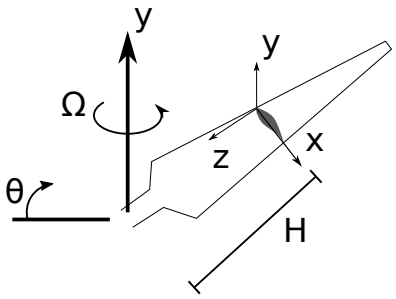

Figure 1. Schematic representation of the reference frame.

$$V_x\frac{\partial V_x}{\partial x}+V_y\frac{\partial V_x}{\partial y}+RoV_z\frac{\partial V_x}{\partial z}+\frac{\partial p}{\partial x}-\frac{1}{Re}\left(\frac{\partial^2 V_x}{\partial x^2}+\frac{\partial^2 V_x}{\partial y^2}+\frac{\partial^2 V_x}{\partial z^2}\right)=2Ro^2V_z-Ro\frac{V_zV_x}{r}, \tag{2}$$

$$V_x\frac{\partial V_y}{\partial x}+V_y\frac{\partial V_y}{\partial y}+RoV_z\frac{\partial V_y}{\partial z}+\frac{\partial p}{\partial y}-\frac{1}{Re}\left(\frac{\partial^2 V_y}{\partial x^2}+\frac{\partial^2 V_y}{\partial y^2}+\frac{\partial^2 V_y}{\partial z^2}\right)=0, \tag{3}$$

$$V_x\frac{\partial V_z}{\partial x}+V_y\frac{\partial V_z}{\partial y}+RoV_z\frac{\partial V_z}{\partial z}+\frac{1}{Ro}\frac{\partial p}{\partial z}-\frac{1}{Re}\left(\frac{\partial^2 V_z}{\partial x^2}+\frac{\partial^2 V_z}{\partial y^2}+\frac{\partial^2 V_z}{\partial z^2}\right)=\frac{1}{Ro}\frac{V_x^2}{r}-2V_x+Ro\,r, \tag{4}$$

The system composed by the dimensional versions of Eq. 1 through 4 was solved using the OpenFOAM, an open source numerical tool for the solution of partial differential equations based on the finite volume method. Central difference discretization scheme was used for the viscous term. The convective terms were discretized with second order upwind scheme (Warming and Beam, 1976). Velocity-pressure coupling was performed by the SIMPLE algorithm with the terms at right-hand side of Eqs. 2 and 4 treated explicitly.

The S809 airfoil, whose geometry is shown in Fig. 2, was simulated at a chord-based Reynolds number of 1 million. This airfoil, designed for wind turbine blades, has a thickness equal to 21% of the chord length (Somers, 1997).

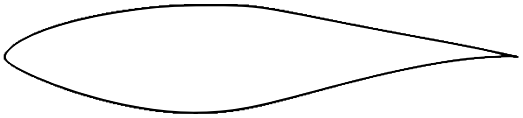

Figure 2. Geometry of the S809 airfoil.

For the discretization of the domain, a C-type mesh was used. The computational domain and details of the mesh in the vicinity of the airfoil are shown in Fig. 3. Solution dependence on the domain and grid refinement was investigated and will be discussed in section 3.1 To prevent difficulties to converge the solution, the source terms of equations 2 and 3 were considered only within the inner portion of the domain (Fig. 3(a)), and Δy=3c was adopted.

Due to its ability to simulate accurately turbulent flows with massive separation, the $k-\omega$ SST model was used to model the effect of the turbulence on the time-averaged flow (Menter, 1994). It combines the $k-\omega$ model (Wilcox, 1988) and the $k-\epsilon$ model (Launder and Spalding, 1974), favoring the former close to no-slip walls and the later for regions distant from walls.

At the domain inlet, fixed values for velocity, turbulent kinetic energy k and specific rate of turbulence dissipation ω was imposed based on wind-tunnel experiments performed at Delft University (Somers, 1997). Fixed pressure was imposed at the outlet boundary, free-slip wall condition was considered for the upper and lower domain boundaries and no-slip wall for the airfoil.

3. RESULTS

3.1 Domain and grid sensitiveness study

To assess the sensitiveness of the solutions to the domain size and to the grid refinement in the sectional plane, a set of two-dimensional simulations were carried out in the range of angle of attack of interest. Figure 4 shows the lift and drag coefficients (C_l and C_d, respectively) predicted with different domain sizes together with wind tunnel measurements by

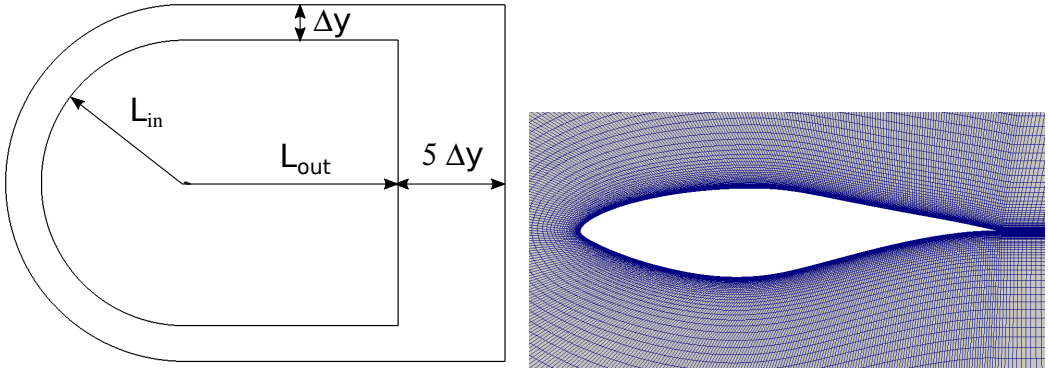

(a) (b)

Figure 3. (a) Computational domain and (b) detail of the mesh close to the airfoil.

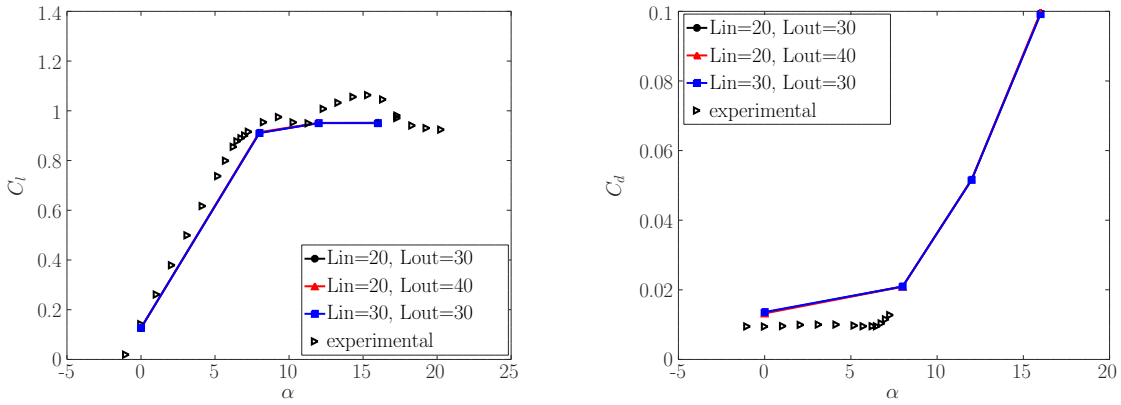

(a) Lift coefficient (b) Drag coefficient

Figure 4. Effect of domain size on (a) lift and (b) drag coefficients for two-dimensional simulations. See Fig. 3(a) for the definition of L_{in} and L_{out}.

Somers (1997). It is seen that the configuration with L_{in}=20c and L_{out}=30c is sufficient to achieve convergence of the results. This domain definition was adopted for the inner portion of the domain in the remaining of the study.

Figure 5 shows the effect of the grid refinement on C_l and C_d. Note that N_x corresponds to the summation of the number of cells on the airfoil surface and twice the number of cells along the downstream region and N_y stands for the number of cells perpendicular to airfoil and wake. Therefore, the total number of cells in each case is $N_x \times N_y$. The solution for an angle of attack α=16°, present in the graphics of Fig. 4, did not converge for most of the tested grids. Therefore, their results are not shown in Fig. 5. For the other conditions, it is seen that the solution with N_x=665 and N_y=119 is independent of the grid refinement to a reasonable degree. In the three-dimensional simulations with α=12°, this grid configuration was used for the planar section. This grid was sufficient to achieve $y^+ < 3$ on the airfoil surface.

From Fig. 4 and 5 it is observed that the drag is generally overpredicted, probably due to the assumption of fully turbulent flow. The lift, on the other hand, is accurately predicted for the three angles of attack considered in the grid dependence study.

3.2 Rotational effect on the separated flow

As reasoned by Gross *et al.* (2012), the present model is not suited to reproduce experimental data. The purpose is to study the flow subjected to some of the rotational effects, namely the ones dominating moderate to high radial positions, considering flow-field variations in the spanwise direction in a periodic manner. However, qualitative comparison of the present simulations with the flow over sections of rotating blades allows us to assess the representativeness of the model.

The flow over the S809 airfoil at angles of attack of 12° and 16° was simulated considering four values for the rotation number, namely, 0, 0.1, 0.2 and 0.4. The local velocity ratio $\Lambda = \Omega R/U = Ro/(c/R)$ was considered to be 1 for all simulations discussed here. This condition correspond to a pure rotation.

As the simulations with α=16° did not converge for some of the grids tested in the section 3.1 they were run with a

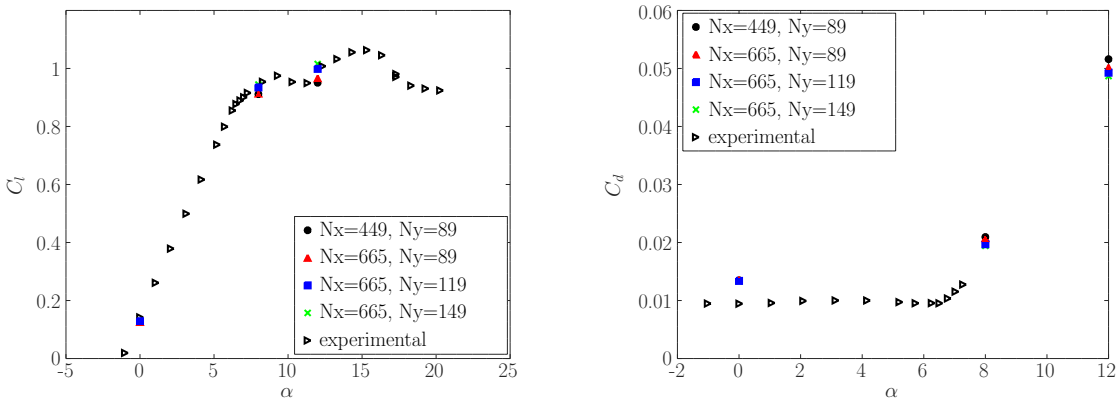

(a) Lift coefficient (b) Drag coefficient

Figure 5. Effect of grid refinement on (a) lift and (b) drag coefficients for two-dimensional simulations.

finer mesh for which N_x=679 and N_y=155 in the inner portion of the domain (see Fig. 3(a)). This mesh resulted in $y^+ <$ 1 on the airfoil surface.

Figures 6 and 7 show variation of lift and drag coefficients as functions of c/R. For $\alpha = 12°$, simulations were carried out with two different domain sizes in the spanwise direction, $L_z = 3c$ and $L_z = 11c$ to assess the sensitivity of the results to this numerical parameter. It is observed that the solutions are fairly independent of the spanwise extent, except for the predicted C_d for $c/R = 0$, which slightly decrease as L_z increases. Moreover, for α =12°, good agreement between results from 3D simulations with c/R=0 and 2D results was achieved. Only the results for $L_z = 3c$ is discussed hereinafter.

As expected, a lift increase with c/R is observed: for $\alpha = 12°$, it increases up to 40% as c/R increases from 0 to 0.4, and for $\alpha = 16°$, more than 60%. On the other hand, the effect of rotation on the sectional drag is not unique. It is common to observe either an increase or a decrease of this force component on sections of wind turbines in comparison to 2D data, and it is frequently argued that the rotational effect on drag depends on the airfoil geometry (Herráez *et al.*, 2014). From the present simulations, as c/R increases, C_d decreases for $\alpha = 12°$ and increases for $\alpha = 16°$. The result for $\alpha = 12°$ is in contrast with measurements performed by the National Renewable Energy Laboratory (NREL), in the United States, on a full scale wind turbine, whose blade sections are based on the same S809 airfoil (Hand *et al.*, 2001). However, for 12° angle of attack, the measured increase in C_d was marginal (Breton *et al.*, 2007). Moreover, it is important to note that the rotational effect on the drag coefficient of a blade section may depend on the wake dynamics (Bangga *et al.*, 2017a).

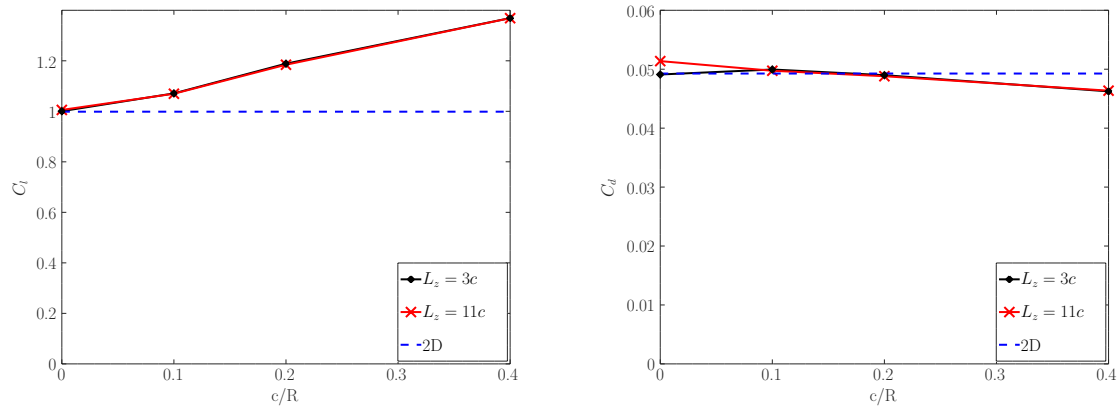

(a) Lift (b) Drag

Figure 6. (a) Lift and (b) drag coefficients as functions of c/R from spanwise homogeneous simulations with different spanwise lengths at an angle of attack α=12°.

The spanwise-averaged pressure coefficient, C_p, distribution on the airfoil surface is show in Fig. 8 together with the chordwise location of the boundary layer separation. The separation line was considered as the locus where the projection of the tangent shear stress onto the sectional plane is zero. As predicted by integral analysis of rotating boundary layer (Du

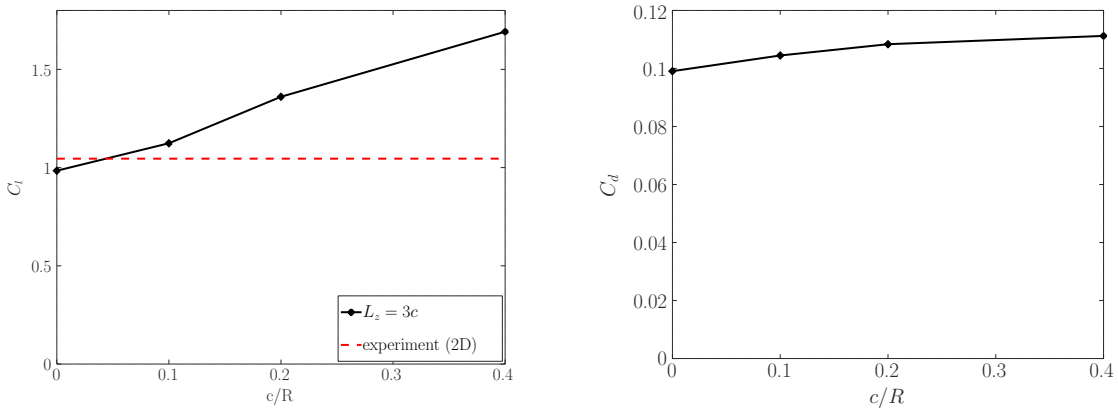

(a) Lift (b) Drag

Figure 7. (a) Lift and (b) drag coefficients as functions of c/R from spanwise homogeneous simulations with different spanwise lengths at an angle of attack α=16°.

and Selig, 2000), the separation line moves towards the trailing edge as the blade hub is approached. It is also observed that, in the region of separated flow, the pressure distribution assumes a triangular shape in the presence of rotational effects, while it is uniform for a translating airfoil. Based on an order of magnitude analysis, Corten (2001) explains that the pressure gradient balance the approximately uniform streamwise Coriolis acceleration in the separated-flow region. This behavior is also observed in experiments (Sicot *et al.*, 2008).

For the two angles of attack, it it seen that the pressure decreases throughout the upper surface as the c/R increases, which is in accordance with the observed lift increase. Moreover, this offer an explanation for the irregular rotational effect on the drag, as observed in Fig. 6(b) and Fig. 7(b). The increased suction on the aft portion of the airfoil, contributes to increase the pressure drag, while the fore portion works to reduce the pressure drag. The global effect is thus dictated by the balance between this two contributions.

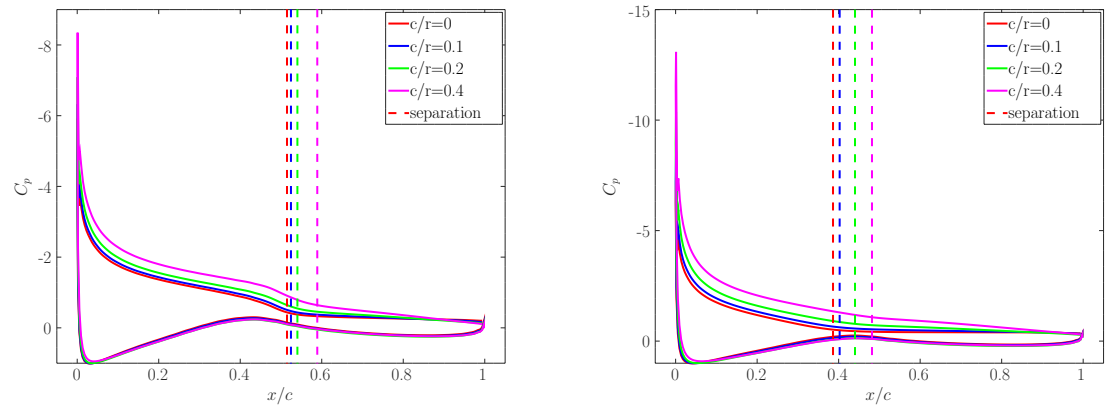

(a) α=12° (b) α=16°

Figure 8. Surface pressure distribution and upper surface separation point for different values of c/R from spanwise homogeneous simulations.

Figure 9 and 10 show the spanwise vorticity field superimposed by the sectional projection of the streamlines. It is observed that the vorticity is predominantly in the attached boundary layer and in the mixing layer between the recirculation and the external irrotational flow. Moreover, it can be seen that as c/R increases the volume of the region of recirculating flow reduces. This reduction is also observed in 3D simulations over rotating blades (Mauro *et al.*, 2017) and will be discussed later in this paper. However, it is important to note that the rotational augmentation at high angles of attack is frequently attributed to this reduction, as it weakens the decamber effect (Bangga *et al.*, 2017b).

The field of the spanwise velocity component w is shown in Figures 11 and 12 together with streamlines that approximate the separating streamlines. It is seen that appreciable values of w are observed in the region of separated flow and its vicinity. This outboard flow deflection is also observed in three-dimensional flow over rotation blades and may be due

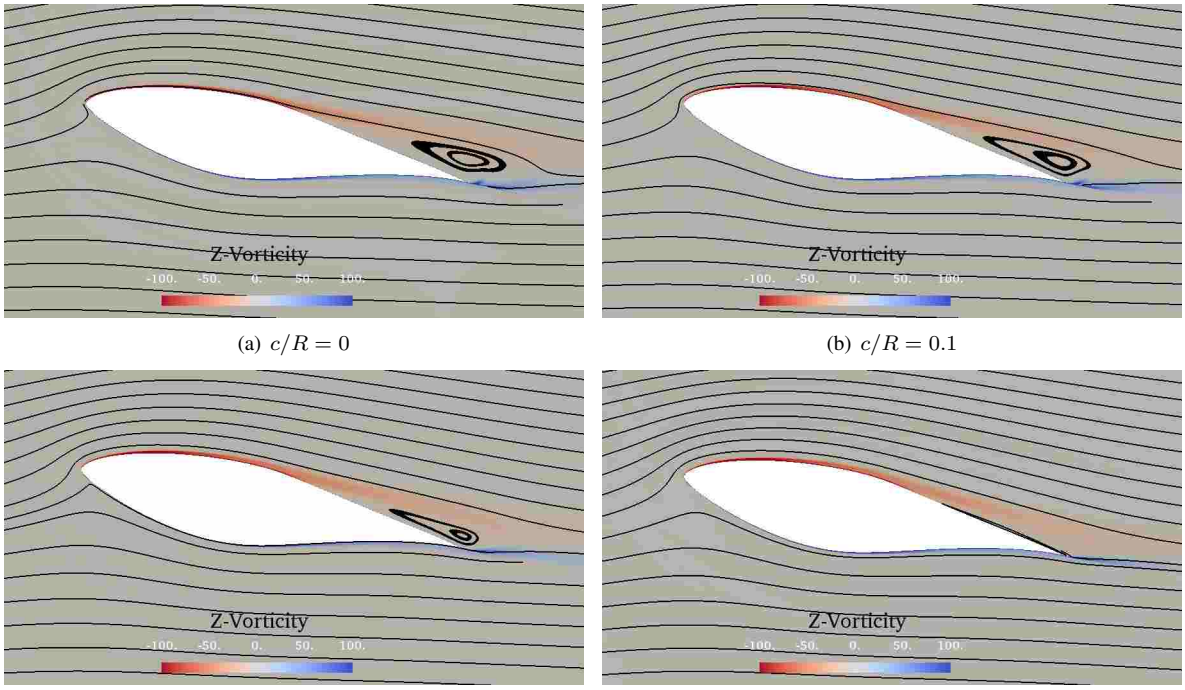

(a) $c/R = 0$ (b) $c/R = 0.1$

(c) $c/R = 0.2$ (d) $c/R = 0.4$

Figure 9. Field of spanwise vorticity superimposed by the sectional projection of the streamlines for $\alpha = 12°$.

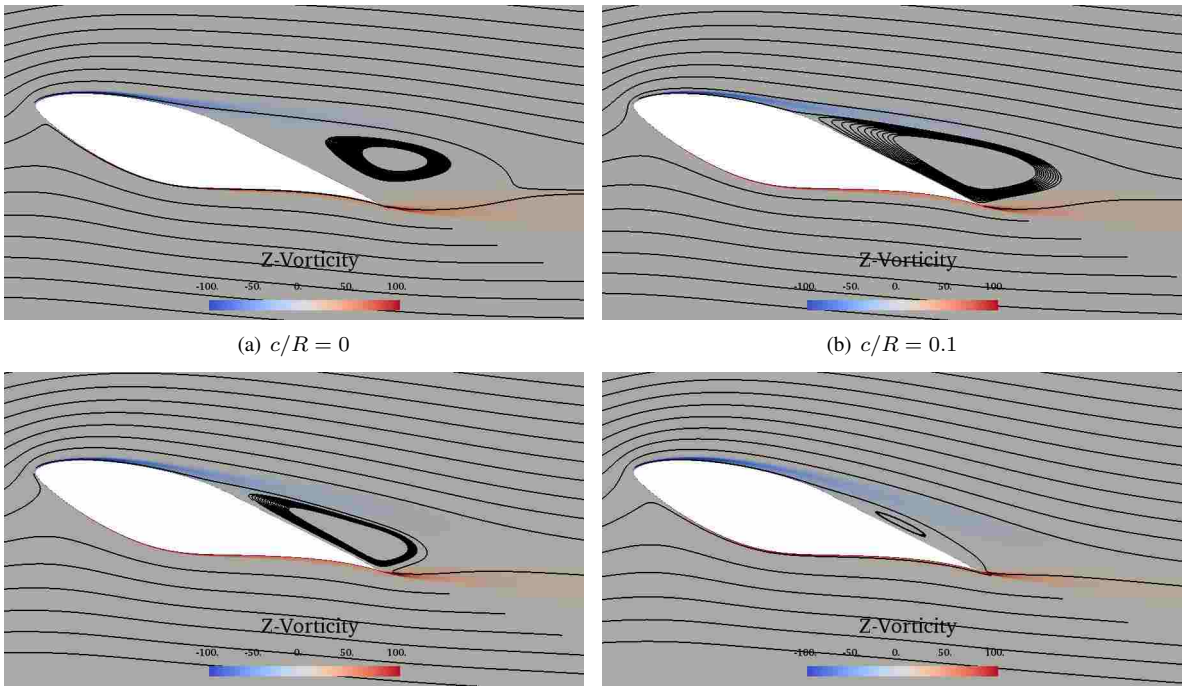

(a) $c/R = 0$ (b) $c/R = 0.1$

(c) $c/R = 0.2$ (d) $c/R = 0.4$

Figure 10. Field of spanwise vorticity superimposed by the sectional projection of the streamlines for $\alpha = 16°$.

to the action of the centrifugal acceleration in the region of low streamwise velocity component u.

We now return to the discussion about the volume of the recirculating bubble. The separating streamlines for different values of c/R are shown in Fig. 13 and evidence the reduction of the bubble as c/R increases for both angles of attack considered. As discussed in section 1, this effect is commonly explained as the consequence of spanwise gradients. However, this effect cannot justify the reduction of the recirculation region for the present results since, as indicated by Fig. 14 and Fig. 15, the flow field is basically uniform in the spanwise direction. Therefore, the present results indicate

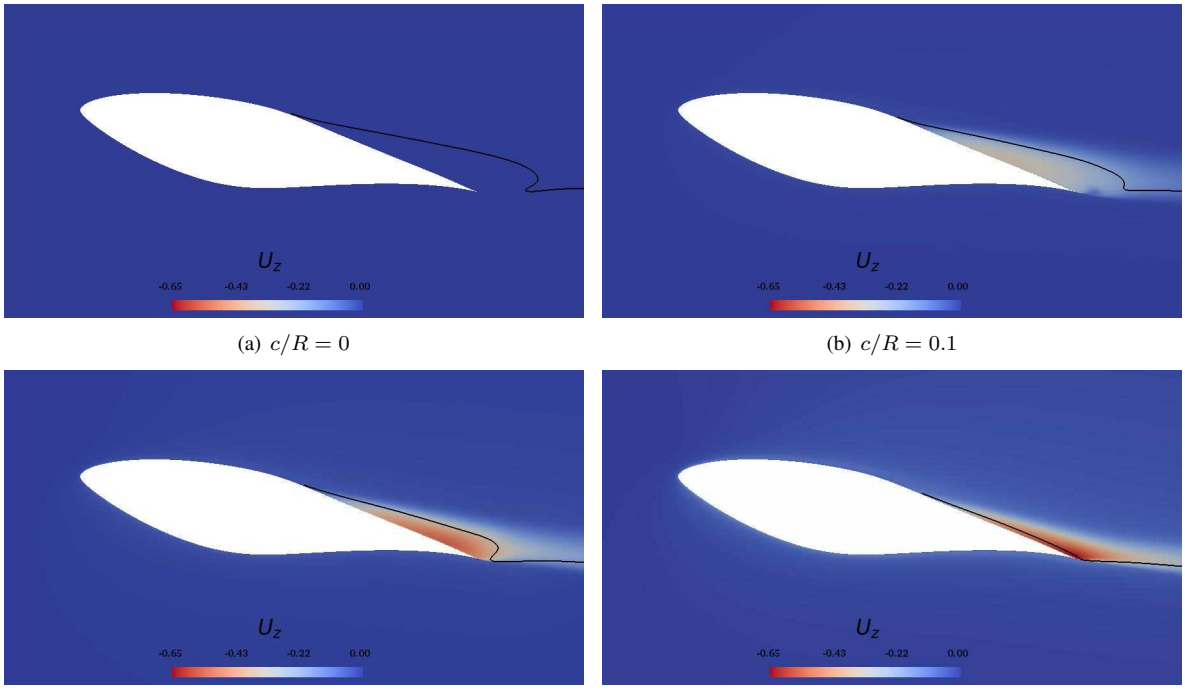

(a) $c/R = 0$ (b) $c/R = 0.1$

(c) $c/R = 0.2$ (d) $c/R = 0.4$

Figure 11. Field of spanwise velocity and sectional projection of the separating streamline for $\alpha = 12°$.

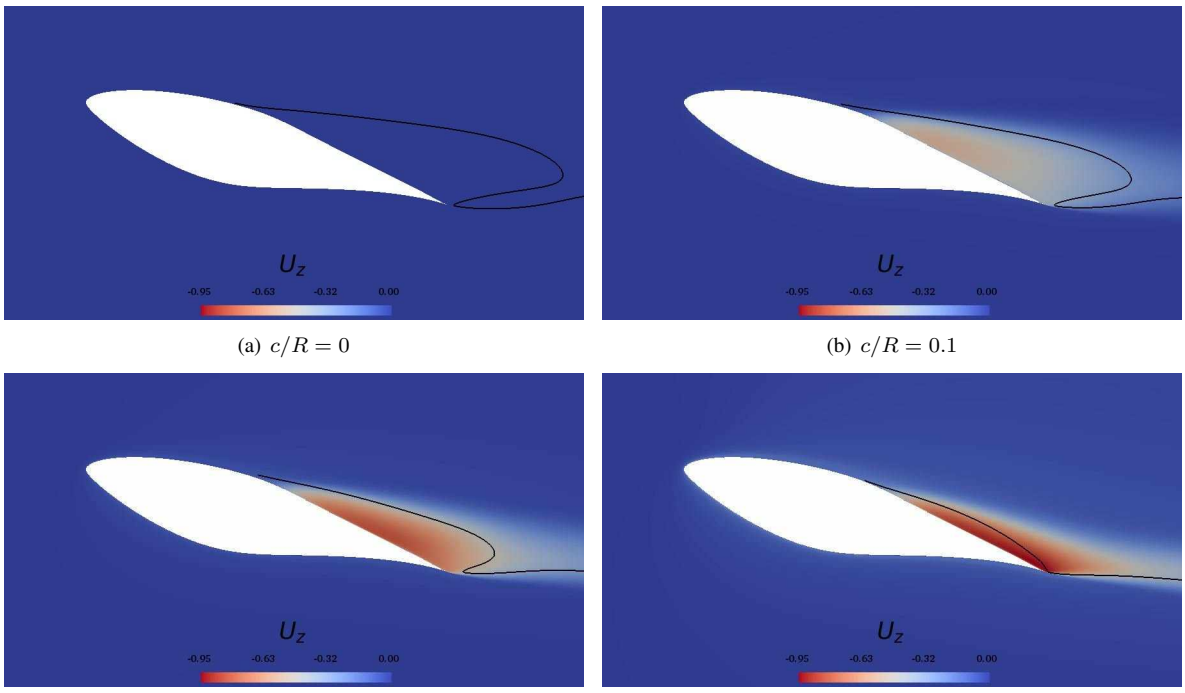

(a) $c/R = 0$ (b) $c/R = 0.1$

(c) $c/R = 0.2$ (d) $c/R = 0.4$

Figure 12. Field of spanwise velocity and sectional projection of the separating streamline for $\alpha = 16°$.

that a mechanism, other than radial drainage of mass and vorticity, may contribute to the reduction of the recirculation region. This observation is in accordance with results by Wojcik and Buchholtz (2014), which indicated that spanwise transport of vorticity is not sufficient to limit the growth of the leading edge vortex of a rotating flat plate at high angle of attack.

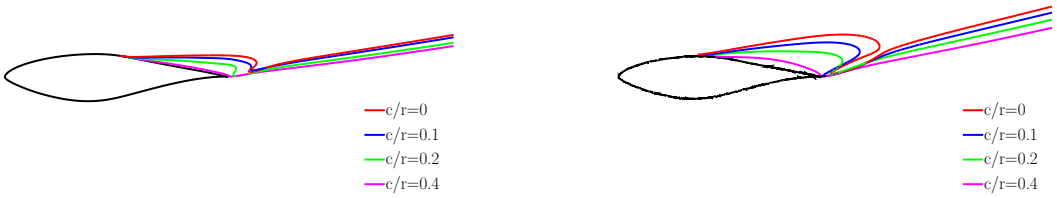

(a) α=12° (b) α=16°

Figure 13. Dividing streamlines for different values of c/R from spanwise homogeneous simulations.

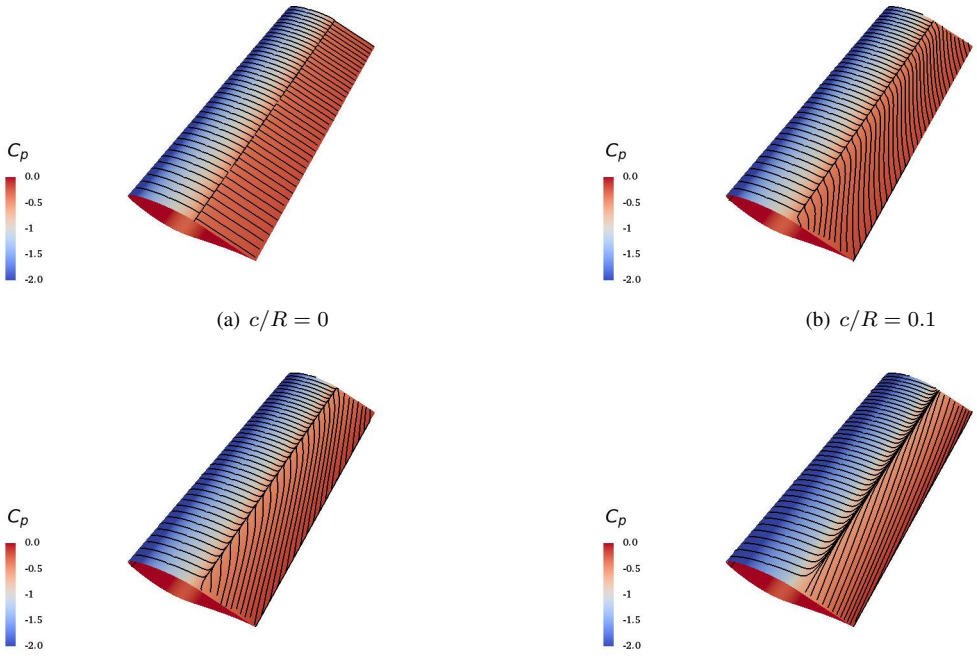

(a) $c/R = 0$ (b) $c/R = 0.1$

(c) $c/R = 0.2$ (d) $c/R = 0.4$

Figure 14. Limiting streamlines and pressure field on the airfoil surface for $\alpha = 12°$.

4. CONCLUSIONS

A spanwise periodic 3D CFD model is used to investigate the effect of rotation on the flow around the section of a wind turbine blade at high angles of attack. The aim is to disregard the effects of global spanwise gradients on the flow physics and is argued to be representative of moderate radial positions. Despite the bold simplifications, the model seem to reproduce important rotational effects observed in sections of rotating wings.

The separation delay predicted by theoretical models based on integral boundary-layer equations is captured by the present simulations. A substantial lift increase is observed as the reference non-dimensional parameter c/R increases. Moreover, the predicted effect of rotation on the drag is rather variable, as observed in three-dimensional simulations and experiments with wind turbine blades. The results suggest that the balance between the effect of the increased suction on the fore and aft portion of the airfoil upper surface dictates whether the rotation increases or reduces the sectional drag coefficient, at least when the 3D effect of the trailing vorticity is neglected.

Interestingly, the model predicted the reduction of the size of the recirculation region, commonly attributed to the centrifugal or radial pumping, which occur due to radial gradients. As for the conditions considered here no appreciable spanwise gradient was observed, is seems that another mechanism, independent of such gradients may contribute to the reduction of the bubble volume.

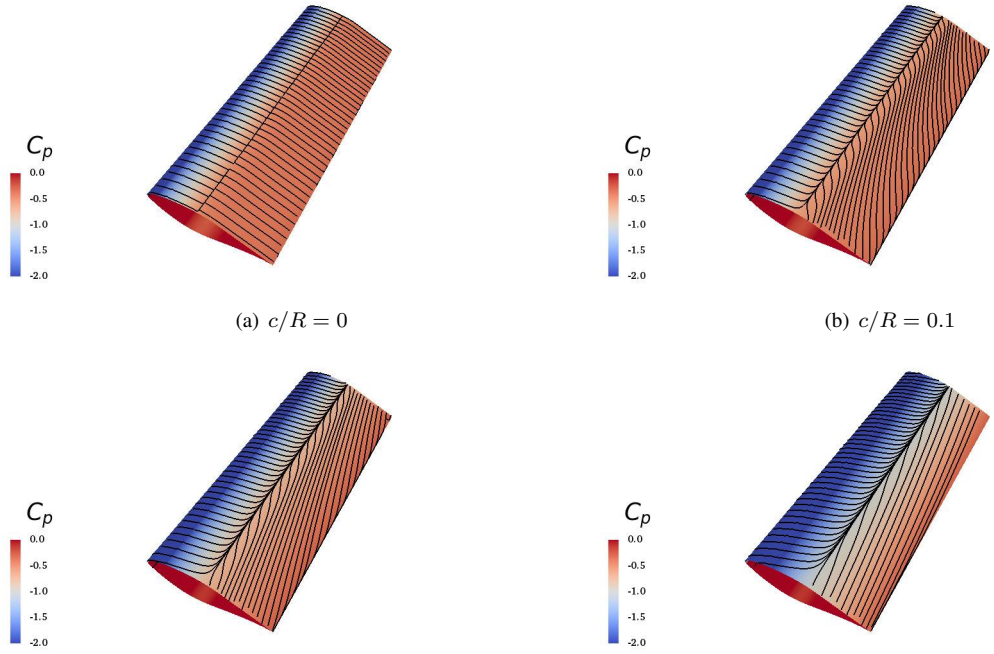

(a) $c/R = 0$ (b) $c/R = 0.1$

(c) $c/R = 0.2$ (d) $c/R = 0.4$

Figure 15. Limiting streamlines and pressure field on the airfoil surface for $\alpha = 16°$.

5. REFERENCES

Bangga, G., Lutz, T., Jost, E. and Krämer, E., 2017a. "CFD studies on rotational augmentation at the inboard sections of a 10MW wind turbine rotor". *Journal of Renewable and Sustainable Energy*, Vol. 9, pp. 1–28.

Bangga, G., Lutz, T. and Krämer, E., 2017b. "Root flow characteristics and 3D effects of an isolated wind turbine rotor". *Journal of Mechanical Science and Thecnology*, Vol. 31, No. 8, pp. 3839–3844.

Banks, W. and Gadd, G., 1963. "Delaying effect of rotation in laminar separation". *AIAA Journal*, Vol. 1, pp. 941–942.

Breton, S., Coton, F. and Moe, G., 2007. "A study on rotational effect and different stall delay models using a prescribed wake vortex scheme and NREL phase VI experiment data". *Wind Energy*, Vol. 11, pp. 459–482.

Carcangiu, C., Soerensen, J., Francesco, C. and Mandas, N., 2007. "CFD-RANS analysis of the rotational effects on the boundary layer of wind turbine blades". *Journal of Physics*, Vol. 75, pp. 1–9.

Chaviaropoulos, P. and Hansen, M., 2000. "Investigating three-dimensional and rotational effects on wind turbine blades by means of quasi-3D Navier-Stokes solver". *Journal of Fluids Engineering*, Vol. 122, pp. 330–336.

Corten, G., 2001. "Flow separation on wind turbine blades". Ultrecht, Netherlands.

Du, Z. and Selig, M., 2000. "The effect of rotation on the boundary layer of a wind turbine". *Renewable Energy*, Vol. 20, pp. 167–181.

Dumitrescu, H., Cardos, V. and Dumitrache, A., 2007. "Modelling of inboard stall delay due to rotaion". *Journal of Physics: Conference Series*, Vol. 75.

Dwyer, H. and McCroskey, W., 1970. "Crossflow and unsteady boundary-layer effects on rotating blades". In *Proceedings of 8th AIAA Aerospace Science Meeting*. Nova Iorque, EUA.

Gross, A., Fasel, H., Friderich, T. and Kloker, M., 2012. "Numerical investigation of rotational augmentation for s822 wind turbine airfoil". *Wind Energy*, Vol. 15, pp. 987–1007.

Hand, M., D., S., Fingersh, L., Jager, D., Cotrell, J.R. Schreck, S. and Larwood, S., 2001. "Unsteady arodynamics experiment phase VI: Wind tunnel test configuration and available data campaigns". Technical report, NREL.

Herráez, I., Stoevesandt, B. and Peinke, J., 2014. "Insight into rotational effects on a wind turbine blade using Navier-Stokes computations". *Energies*, Vol. 7, pp. 6798–6822.

Hu, D., Hua, O. and Du, Z., 2006. "A study on stall-delay for horizontal axis wind turbine". *Renewable Energy*, Vol. 31, pp. 821–836.

Jardin, T., 2017. "Coriolis effect and the attachment of the leading edge vortex". *Journal of Fluid Mechanics*, Vol. 820, p. 312£340.

Jardin, T. and David, L., 2014. "Spanwise gradients in flow speed help stabilize leading-edge vortices on revolving wings". *Physical Review E*, Vol. 90, No. 1, p. 312£340.

Lanzafame, R., Mauro, S. and Messina, M., 2015. "Evaluation of the radial flow effects on micro HAWTs through the use of transition CFD 3D model - PART II: Post-processing and comparison of the results". *Energy Procedia*, Vol. 82, pp. 164–171.

Launder, B. and Spalding, D., 1974. "The numerical computation of turbulent flows". *Computer Methods in Applied Mechanics and Engineering*, Vol. 3, pp. 269–289.

Mauro, S., Lanzafame, R. and Messina, M., 2017. "An insight into the rotational augmentation on HAWTs by means of CFD simulations - PART II: Post processing and force analysis". *International Journal of Applied Engineering Research*, Vol. 12, No. 21, pp. 10505–10529.

Menter, F.R., 1994. "Two-equation eddy-viscosity turbulence models for engineering applications". *AIAA Journal*, Vol. 32, No. 8, pp. 1598–1605.

Narramore, J. and Vermeland, R., 1992. "Navier-Stokes calculations of inboard stall delay due to rotation". *Journal of Aircraft*, Vol. 29, No. 1, pp. 73–78.

Ronsten, G., 1992. "Static pressure measurements on a rotating and a non-rotating 2.375 m wind turbine blade. Comparison with 2D calculations". *Journal of Wind Engineering and Industrial Aerodynamics*, Vol. 39, pp. 105–118.

Schreck, S. and Robinson, M., 2003. "Boundary layer state and flow field structure underlying rotational augmentation of blade aerodynamic response". *Transactions of the ASME*, Vol. 125, pp. 448–456.

Schreck, S., Soerensen, N. and Robinson, M., 2007. "Aerodynamic structures and processes in rotationally augmented flow fields". *Wind Energy*, Vol. 10, pp. 159–178.

Sicot, C., Devinant, P., Loyer, S. and Hureau, J., 2008. "Rotational and turbulence effect on a wind turbine blade. Investigation of the stall mechanisms". *Journal of Wind Engineering and Industrial Aerodynamics*, Vol. 96, pp. 1320–1331.

Somers, D.M., 1997. "Design and experimental resultos for the S809 airfoil". Technical report, NREL.

Warming, R. and Beam, R.M., 1976. "Upwind second-order difference schemes and applications in aerodynamic flows". *AIAA Journal*, Vol. 14, No. 9, pp. 1241–1249.

Wilcox, D., 1988. "Reassessment of the scale-determining equation for advanced turbulence models". *AIAA Journal*, Vol. 26, No. 11, pp. 1299–1310.

Wojcik, C. and Buchholtz, J., 2014. "Vorticity transport in the leading-edge vortex on a rotating blade". *Journal of Fluid Mechanics*, Vol. 743, pp. 249–261.

Zhang, Y. and Deng, S., 2019. "RANS and DDES simulations of a horizontal-axis wind turbine under stalled flow condition using OpenFOAM". *Energy*, Vol. 3, pp. 1155–1163.

6. RESPONSIBILITY NOTICE

The authors are solely responsible for the printed material included in this paper.